Thermal behavior of localized surface plasmon resonance of Au/TiO_2 core/shell nanoparticle arrays

Yue Bing Zheng and Tony Jun Huang[a)]
Department of Engineering Science and Mechanics, Pennsylvania State University, University Park, Pennsylvania 16802

Amit Yogesh Desai, Shi Jie Wang, Lee Kheng Tan, Han Gao, and Alfred Cheng Hon Huan
Institute of Materials Research and Engineering, 3 Research Link, Singapore 117602, Singapore

(Received 26 January 2006; accepted 11 April 2007; published online 3 May 2007)

The authors investigate the thermal behavior of localized surface plasmon resonance (LSPR) of Au/TiO_2 core/shell nanoparticle arrays. Thermal annealing is carried out in three different routes, i.e., pre-TiO_2 annealing, post-TiO_2 annealing, and combinational annealing. It is found that the pre-TiO_2 annealing causes a blueshift in LSPR, the combinational annealing results in a redshift, and the post-TiO_2 annealing leads to an initial blueshift, followed by a redshift, and finally reverts to a blueshift. These resonance shifts correlate well with morphologic changes in Au cores and crystallization of TiO_2 shells revealed by atomic force microscopy, x-ray diffraction, and x-ray photoemission spectroscopy. © *2007 American Institute of Physics*. [DOI: 10.1063/1.2736283]

Recently there has been considerable interest in investigating localized surface plasmon resonance (LSPR) of metallic nanostructures. This is primarily due to the promise in developing integrated plasmonic devices that are capable of manipulating light on the nanoscale.[1–3] LSPR arises from the collective oscillation of electrons on metallic nanostructures.[4] The shape and position of LSPR are highly sensitive to nanostructures' sizes, shapes, spacings, and environments.[5–7] Among various metallic nanostructures, core/shell nanoparticles exhibit high LSPR tunability and applicability in areas such as surface-enhanced Raman spectroscopy and biosensing.[8–10] In this letter, we report our investigation of the thermal behavior of LSPR of Au/TiO_2 core/shell nanoparticle arrays. We have employed a variety of characterization tools, including ultraviolet-visible spectrophotometer (UVS), atomic force microscopy (AFM), x-ray diffraction (XRD), and x-ray photoemission spectroscopy (XPS), to reveal the impacts associated with the various mechanisms involved in the annealing processes.

Au nanoparticle arrays were fabricated on glass substrates using nanosphere lithography.[11] Monolayers of polystyrene (PS) nanospheres (300 nm in diameter) were used as masks, and Au (~35 nm in thickness) and Cr (~5 nm in thickness, as an adhesive layer) were deposited through electron-beam evaporation. Triangular Au nanoparticles were produced on the substrates after selective removal of PS nanospheres. Conformal TiO_2 shells of controlled thickness were deposited onto the Au surfaces to form Au/TiO_2 core/shell nanoparticles using a homemade atomic layer deposition (ALD) system.[12] In the Au/TiO_2 core/shell nanoparticles, TiO_2 were only coated onto the Au surfaces exposed to the deposition, and there was no TiO_2 coating on bases of the particles that were in contact with substrates. For LSPR measurements, the extinction spectra of nanoparticle arrays were recorded on a Shimazu UVS. AFM images were taken on a Digital Instrument Nanoscope III microscope. XRD θ-2θ scans were recorded using a GADDS XRD system. XPS measurements were performed on a VG ESCALAB 220i-XL system with a monochromatic Al $K\alpha$ source (1486.6 eV). The pass energy of the XPS analyzer was set at 10 eV to achieve high accuracy.

Thermal annealing processes were carried out in a furnace under ambient conditions at a series of temperatures up to 600 °C. Each annealing process was conducted for 1 h at the desired temperature. Three different annealing routes were employed, producing three groups of samples, i.e., the as-deposited and thermal annealed Au nanoparticle arrays (pre-TiO_2 annealing), the as-deposited and thermal annealed Au/TiO_2 core/shell nanoparticle arrays (post-TiO_2 annealing), and the as-deposited and thermal annealed Au/TiO_2 core/shell nanoparticle arrays with their Au cores preannealed at 600 °C before the deposition of TiO_2 (combinational annealing).

Figure 1 shows a set of extinction spectra for the pre-TiO_2 annealing samples. We observe that the as-deposited Au nanoparticles exhibited a broad LSPR band with weak

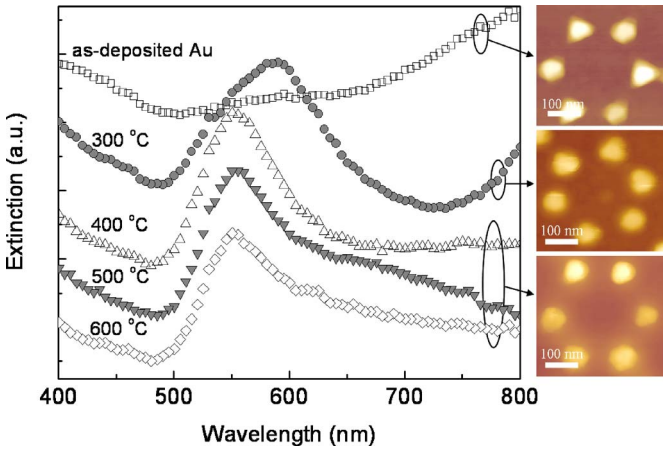

FIG. 1. Set of extinction spectra for the as-deposited and annealed Au nanoparticle arrays (pre-TiO_2 annealing samples). The spectra were shifted vertically for clarity. This was accompanied by AFM images of Au nanoparticles annealed at different temperatures. The third AFM image was taken from the sample annealed at 400 °C and was similar to the images from samples annealed at 500 and 600 °C.

[a)]Electronic mail: junhuang@psu.edu

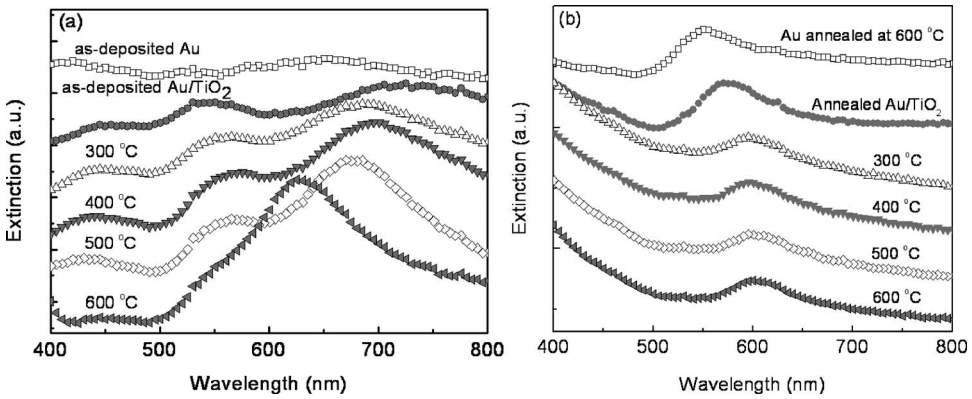

FIG. 2. Set of extinction spectra for (a) the as-deposited and annealed Au/TiO_2 core/shell nanoparticle arrays (post-TiO_2 annealing samples) and (b) the as-deposited and annealed Au/TiO_2 core/shell nanoparticle arrays with Au cores preannealed at 600 °C before the deposition of TiO_2 (combinational annealing samples). The spectra were shifted vertically for clarity.

peak intensity. The observed broad LSPR band arises from the broad size distribution and morphology discrepancy among the as-deposited Au nanoparticles. As confirmed in the accompanied AFM image for the as-deposited samples, the triangular nanoparticles exhibited differences in both shape and dimension. When the sample was annealed at 300 °C, its LSPR bandwidth decreased to ~2/3 of the as-deposited nanoparticles and showed an obvious increase of intensity. The band can be identified as the in-plane dipole resonance.[13] The decrease of bandwidth and increase of intensity are attributed to the reduced discrepancy of morphologies and dimensions among Au nanoparticles after the annealing process. The AFM images in Fig. 1 show that the as-deposited triangular Au nanoparticles became more circular after annealing at 300 °C. The shape change arose from the sample's tendency to minimize its surface free energy and transform into a more stable spherical shape. This shape transformation also resulted in a blueshift of the LSPR band, consistent with the electrodynamic theory and experimental results from other Au nanostructures.[13,14] As shown in Fig. 1, further annealing of the sample at 400 °C completed the transformation of the triangular Au nanoparticles into spherical nanoparticles, continued to blueshift and increase the intensity of the LSPR band, and halved the bandwidth in comparison to the as-deposited nanoparticles. Further annealing of the sample at higher temperatures (500 or 600 °C) induced no obvious change in the LSPR band. This observation is reiterated by the AFM results which depict no differences among Au nanoparticles being annealed at 400, 500, or 600 °C.

Figure 2 reveals the effects of thermal annealing on LSPR of Au/TiO_2 core/shell nanoparticle arrays. TiO_2 shells of ~36 nm in thickness were deposited on top of the Au surfaces and the extinction spectra of the post-TiO_2 annealing samples are shown in Fig. 2(a). Upon the deposition of TiO_2 shells, the single broad band of the as-deposited Au nanoparticles splits into two LSPR bands. By comparing the experimental spectrum with theoretical results obtained from discrete dipole approximation calculations, the left band with the peak λ_{LSPR} at 547 nm is assigned to the in-plane quadrupole resonance, and the right band with the peak λ_{LSPR} at 728 nm arises from the in-plane dipole resonance.[13] Annealing the sample at 300 °C resulted in a blueshift of the right band and a redshift of the left band. In contrast, annealing the sample at 400 °C resulted in a redshift of the right band while the left band remained stationary. When the sample was annealed at 500 °C, the right band reverted to a blueshift and the left band kept still. Further annealing the sample at 600 °C resulted in a continued blueshift of the right band. In contrast, the left band shrank and merged into the shoulder of the right band. With each increase in the annealing temperature, the right band became more narrow and intense. In contrast to the post-TiO_2 annealing samples, only a single band from the in-plane dipole resonance was found in the spectra of the combinational annealing samples [Fig. 2(b)]. The deposition of TiO_2 shells resulted in a redshift of the LSPR band without obvious change in the band shape. As the annealing temperature increased, the LSPR band continued to redshift. Although annealing the sample at 300 °C broadened the bandwidth and deceased the intensity, higher annealing temperatures induced no additional changes to the samples' band shape.

While the thermal behavior of the Au nanoparticles (pre-TiO_2 annealing samples) can be explained by the changes in the morphologies and dimensions of the nanoparticles, the behavior of the Au/TiO_2 core/shell nanoparticles (post-TiO_2 annealing and combinational annealing samples) is not as straightforward. To understand the physical mechanisms behind the thermal behavior of the Au/TiO_2 core/shell nanoparticles, XRD and XPS characterizations were conducted. XRD θ-2θ scans were recorded on both samples of Au nanoparticles and Au/TO_2 core/shell nanoparticles. Both XRD spectra (data not shown) exhibited similar Au peaks, indicating that no phase change occurred to Au during the annealing processes. Because the signals from the thin TiO_2 shells were relatively weak and overlapped with the background signals from glass substrates, we could not observe TiO_2 peaks in the XRD spectrum of the core/shell nanoparticles. In order to investigate the effects of thermal annealing on the TiO_2 crystal structures, thicker TiO_2 films were grown on silicon substrates. Figure 3(a) shows the XRD spectra for TiO_2 films annealed at a series of temperatures. We can see that the as-grown TiO_2 was amorphous and it developed into a poly-

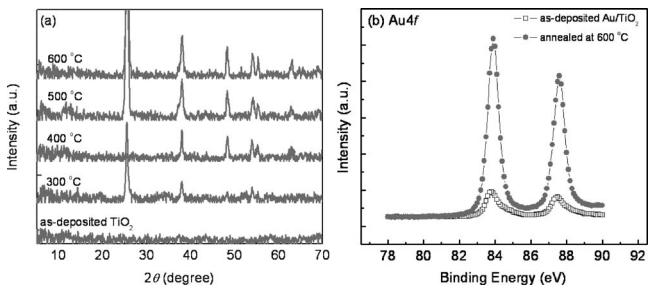

FIG. 3. (a) XRD spectra for TiO_2 thin films annealed at a series of temperatures; (b) Au 4*f* core-level XPS spectra for the as-deposited and annealed Au/TiO_2 core/shell nanoparticle arrays before and after the annealing process at 600 °C.

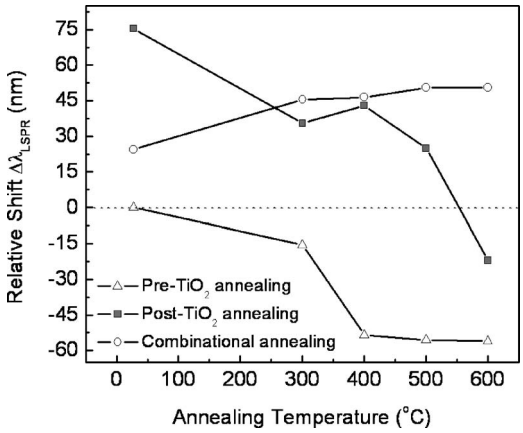

FIG. 4. Relative shifts of the LSPR band peak (the in-plane dipole resonance) as a function of the annealing temperature.

crystalline anatase structure after being annealed at 300 °C. Further annealing at higher temperatures enlarged the crystalline domains, as evidenced from the increased XRD peak intensity shown in Fig. 3(a).

Figure 3(b) shows the Au 4*f* XPS spectra of the Au/TiO_2 core/shell nanoparticles (post-TiO_2 annealing samples) before and after being annealed at 600 °C. TiO_2 of ~5 nm in thickness was chosen here to allow both Au and TiO_2 signals to be detected by XPS. We can see that the Au 4*f* signal intensity increased significantly after the annealing process. A very small shift was found in the location of the peak of the spectra, indicating that no obvious chemical reaction occurred to Au. Since we did not observe obvious cracks or increased surface roughness on TiO_2 after the annealing process, we believe that the detected increase in Au 4*f* signal intensity is a result of Au diffusing into TiO_2. This hypothesis is consistent with the observed Ti 2*p* intensity decrease (data not shown) after the annealing process. We also observed that the Ti 2*p* spectrum shifted towards a higher binding energy after the annealing process; this shift is attributed to the decreased oxygen vacancy concentration in TiO_2 at higher temperatures.[15]

We further quantified the relative shifts of the LSPR band peaks (the in-plane dipole resonance) as a function of annealing temperature for the three groups of samples, i.e., pre-TiO_2 annealing, post-TiO_2 annealing, and combinational annealing (Fig. 4). In the combinational annealing samples, the pre-TiO_2 annealing of the Au cores at 600 °C resulted in the formation of stable spherical nanoparticles and Au morphologies and dimensions remained unchanged during the subsequent post-TiO_2 annealing process. The shape stability of the preannealed Au cores in the presence of TiO_2 shells was verified by AFM analysis (data not shown). On the other hand, the TiO_2 crystal structure has changed from amorphous to polycrystalline anatase after the annealing process and the refractive indices of the ALD deposited amorphous and anatase TiO_2 thin films were measured to be 2.2 and 2.65, respectively.[16] Assuming that isolated spherical Au nanoparticles were embedded in homogeneous TiO_2 materials, we conducted theoretical calculations based on the Mie theory.[17] By simply considering the change in the refractive index of TiO_2, a trend similar to the experimental results for the combinational annealing samples (Fig. 4) was obtained, indicating that the TiO_2 crystallization is the dominant mechanism for the observed redshift in the combinational annealing samples. In contrast to the pre-TiO_2 annealing and combinational annealing samples, the post-TiO_2 annealing samples exhibited a blueshift first, then a redshift, and finally reverted to a blueshift. This observed zigzag shift is likely a result of the interplay between two different mechanisms during the annealing processes: the morphologic change in the Au cores caused a blueshift and the crystallization of the TiO_2 shells resulted in a redshift. AFM characterizations (data not shown) revealed that the thermal-induced shape transformation of Au was slower in the Au/TiO_2 core/shell nanoparticles than in the Au nanoparticles; this observation correlates with our observation that at higher annealing temperatures (500 and 600 °C) the LSPR in the post-TiO_2 annealing samples continued to blueshift while that in the pre-TiO_2 annealing samples remained constant.

In summary, we have investigated the thermal behavior of LSPR of Au/TiO_2 core/shell nanoparticle arrays. Annealing processes transformed triangular Au nanoparticles into spherical ones. The thermal-induced shape transformation of Au was observed to be slower in the core/shell Au/TiO_2 nanoparticles than the Au nanoparticles. The crystallization of TiO_2 shells occurred during the annealing process and led to higher refractive index of TiO_2. Based on the characterization results from UVS, AFM, XRD, and XPS, we found that the morphologic changes in Au cores and the crystallization of TiO_2 shells are the dominant mechanisms for the observed blueshift in the pre-TiO_2 annealing samples, redshift in the combinational annealing samples, and zigzag shift in the post-TiO_2 annealing samples.

We gratefully acknowledge Bala Krishna Juluri, John Waldeisen, and Xiaole Mao for their help with the manuscript. This work was supported by the NSF NIRT grant (ECCS-0609128) and the start-up fund provided by The Pennsylvania State University.

[1] N. Fang, H. Lee, C. Sun, and X. Zhang, Science **308**, 534 (2005).
[2] H. J. Lezec, A. Degiron, E. Devaux, R. A. Linke, L. Martin-Moreno, F. J. Garcia-Vidal, and T. W. Ebbesen, Science **297**, 820 (2002).
[3] E. Ozbay, Science **311**, 189 (2006).
[4] E. Hutter and J. H. Fendler, Adv. Mater. (Weinheim, Ger.) **16**, 1685 (2004).
[5] W. A. Murray, J. R. Suckling, and W. L. Barnes, Nano Lett. **6**, 1772 (2006).
[6] Y. G. Sun and Y. N. Xia, Science **298**, 2176 (2002).
[7] H. Wang, D. W. Brandl, F. Le, P. Nordlander, and N. J. Halas, Nano Lett. **6**, 827 (2006).
[8] A. J. Haes and R. P. Van Duyne, Anal. Bioanal. Chem. **379**, 920 (2004).
[9] A. J. Haes, C. L. Haynes, A. D. McFarland, G. C. Schatz, R. P. Van Duyne, and S. L. Zou, MRS Bull. **30**, 368 (2005).
[10] B. Pettinger, B. Ren, G. Picardi, R. Schuster, and G. Ertl, Phys. Rev. Lett. **92**, 096101 (2004).
[11] J. C. Hulteen and R. P. Van Duyne, J. Vac. Sci. Technol. A **13**, 1553 (1995).
[12] M. S. Sander, M. J. Cote, W. Gu, B. M. Kile, and C. P. Tripp, Adv. Mater. (Weinheim, Ger.) **16**, 2052 (2004).
[13] R. C. Jin, Y. C. Cao, E. C. Hao, G. S. Metraux, G. C. Schatz, and C. A. Mirkin, Nature (London) **425**, 487 (2003).
[14] W. Y. Huang, W. Qian, and M. A. El-Sayed, J. Appl. Phys. **98**, 114301 (2005).
[15] Y. B. Zheng, S. J. Wang, A. C. H. Huan, C. Y. Tan, L. Yan, and C. K. Ong, Appl. Phys. Lett. **86**, 112910 (2005).
[16] J. Aarik, A. Aidla, A. A. Kiisler, T. Uustare, and V. Sammelselg, Thin Solid Films **305**, 270 (1997).
[17] G. Mie, Appl. Phys. Lett. **25**, 377 (1908).